Probing the concept of line tension down to the nanoscale

Romain Bey, Benoit Coasne, Cyril Picard

Probing the concept of line tension down to the nanoscale

Romain Bey,[1] Benoit Coasne,[1, a)] and Cyril Picard[1, b)]
Univ. Grenoble Alpes, CNRS, LIPhy, 38000 Grenoble, France

(Dated: February 3, 2020)

A novel mechanical approach is developed to explore by means of atom-scale simulation the concept of line tension at a solid-liquid-vapor contact line as well as its dependence on temperature, confinement, and solid/fluid interactions. More precisely, by estimating the stresses exerted along and normal to a straight contact line formed within a partially wet pore, the line tension can be estimated while avoiding the pitfalls inherent to the geometrical scaling methodology based on hemispherical drops. The line tension for Lennard-Jones fluids is found to follow a generic behavior with temperature and chemical potential effects that are all included in a simple contact angle parameterization. Former discrepancies between theoretical modeling and molecular simulation are resolved, and the line tension concept is shown to be robust down to molecular confinements. The same qualitative behavior is observed for water but the line tension at the wetting transition diverges or converges towards a finite value depending on the range of the solid/fluid interactions at play.

I. INTRODUCTION

The contact line between three phases is a particular *locus* conducive to physical couplings between the macroscopic and the molecular scales. Diverse phenomena are intrinsically bound to the presence of a contact line, such as heterogeneous nucleation[1–3], formation of nanovesicles from a membrane[4], dynamical wetting[5–7], and as a last example among others stabilisation and pinning of nanoinclusions at an interface (bubbles, droplets, colloids, etc.)[8–10]. To better understand these phenomena, which play a key role in several applicative fields such as biotechnology (nanoemulsion, encapsulation)[11], chemical engineering (catalysis, electrochemistry)[12] or process engineering (boiling, condensation)[13], a challenge remains in deciphering the effects due to the presence of a contact line. At the micron scale, the wedge that is formed in the vicinity of a solid/liquid/vapor contact line may be responsible for enhanced heat and mass transfer at the origin for instance of the well known coffee ring effect[14]. At the nanometer scale, such a wedge has been identified to give rise to specific molecular interactions close to the three-phase contact line, at the origin of a specific free energy contribution: the line tension[15–17]. This specific thermodynamical quantity was first mentioned by Gibbs[18], who introduced the line tension τ as an excess free energy per unit length of contact line or a tangential force along this line. Unlike surface tension of planar fluid/fluid interfaces, line tension can be either positive or negative as there is no thermodynamical argument to predict its sign[19]. From simple scaling arguments, the order of magnitude of τ for water is expected to be $|\tau| \sim \gamma_{lv}\sigma \sim 20$ pN with γ_{lv} the liquid/vapor surface tension and σ the molecular size[1]. Such a scaling implicitly suggests that the impact of line tension is limited to the molecular scale[16]. Nevertheless, in the case of nanostructured materials, the effect of line tension can be scaled up and impact macroscopic phenomena. For instance, it has been recently shown that line tension could control the macroscopic bulk pressure required to induce capillary drying within hydrophobic nanoporous material[1,3].

Despite its wide range of possible contributions, the understanding of line tension is still limited. Available measurements, either from experiments[20–26] or based on numerical simulations[17,27–30], lead to mostly negative but also positive values for the line tension with magnitude spanning from 10^{-6} to 10^{-12} N, this dispersion being probably due to the diversity of methods and systems under investigation[31]. Moreover, from analytical predictions of Joanny and De Gennes, a divergence of line tension towards infinite positive values is expected for Lennard-Jones fluids at the wetting transition[15]. From this variability of τ, one must admit that estimating accurately line tension remains a delicate task with long-standing debates about the role of competing effects, such as line pinning[22] or surface curvature corrections[32–34]. Up to date, no consensus has been met on the dependence of line tension on physical parameters such as temperature, substrate hydrophilicity or fluid molecular structure.

Most experimental and molecular simulation measurements of line tension consist of evaluating the dependence of the contact angle θ of a sessile drop on the radius r of its circular contact line. In this approach, a simple decomposition into surface and line free energies reveals that a geometrical scaling, known as the modified Young equation, is expected[35]:

$$\cos\theta = \cos\theta_Y - \frac{\tau}{\gamma_{lv} r} \tag{1}$$

where $\cos\theta_Y = (\gamma_{sv} - \gamma_{sl})/\gamma_{lv}$ is the Young contact angle defined from the solid-vapor γ_{sv}, solid-liquid γ_{sl} and liquid-vapor γ_{lv} surface tensions. Eq. [1] implicitly assumes that surface and line tensions only depend on the nature of the materials so that changes in $\cos\theta$ are proportional to $1/r$. However, surface and line tensions can vary with the fluid chemical potential as well as with surface and line curvatures[35,36]. In this respect, while

a)Electronic mail: benoit.coasne@univ-grenoble-alpes.fr
b)Electronic mail: cyril.picard@univ-grenoble-alpes.fr

curvature seems to have a negligible impact on γ_{lv} (expressed with the so-called Tolman length) down to submolecular sizes, its effect on line tension remains to be established[33,34]. Moreover, the geometrical approach in Eq. [1] suffers from difficulties in evaluating the shape of the sessile drop. In particular, experimental departures from Eq. [1][22,24] cast doubt on the relevance of the geometrical scaling methodology to measure line tensions τ[34,36,37]. Even in molecular simulation approaches, the position of interfaces and lines is ambiguous at the molecular scale so that line tensions estimated numerically are subjected to large error bars.

In this paper, a molecular simulation methodology is developed to estimate line tensions τ without geometrical scaling. The effects of temperature, confinement, solid/fluid interactions, and chemical potential are investigated for any dispersive fluid modeled by a Lennard-Jones potential (LJ) and for water. In the spirit of the seminal work of Tarazona[38] and recent approach of Shao et al[39], statistical mechanics expressions are used to determine τ from the stress anisotropy in the vicinity of a triple line. While the approach of Shao et al[39] is mostly applicable to three fluid systems with limited interface curvature, our approach addresses the case of two fluids confined between solid walls (Fig. 1) without any restriction on the curvature of the fluid/fluid interface, that is for any contact angle and any confinement. In this approach, a liquid in contact with its vapor is confined, at a temperature T, in a slit pore of a width h formed by two solid planar walls perpendicular to the z direction (Fig. 1). The system is infinite in the x and y directions thanks to the use of periodic boundary conditions (see methodological details in *Materials and Methods* and *Supplementary Information*).

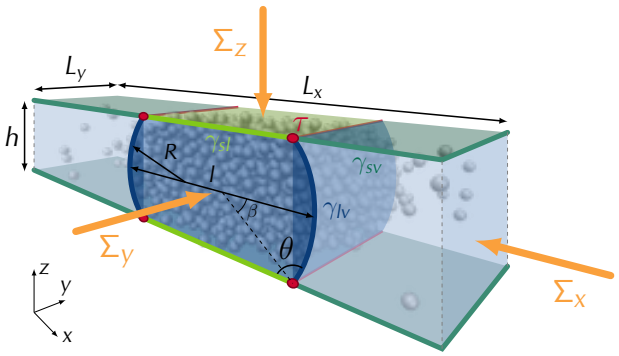

Figure 1. Set-up consisting of a liquid in contact with its vapor confined between two solid walls (perpendicular to the z direction). Solid/fluid interfaces are separated by a distance h. Periodic boundary conditions are applied along the x and y directions which are parallel and perpendicular to the red contact lines. The line tension τ of these straight contact lines is estimated from the forces Σ_x, Σ_y and Σ_z exerted along x, y and z.

Our approach avoids the delicate computation of local stresses or pressures at the vicinity of the contact line. The value of τ is directly extracted from the measurement of total forces Σ_x, Σ_y and Σ_z in the three space directions. This approach is used to probe the line tension of the contact line of a Lennard-Jones fluid or water within various confinements.

II. MATERIAL AND METHODS

A. A mechanical route to measure line tension

At mechanical equilibrium the total force Σ_x exerted on the fluid system through a yz plane does not depend on the x location of the plane. For a plane within the vapor phase far from the liquid phase, Σ_x relies on the vapor pressure P_v and the solid-vapor surface tension γ_{sv} while for a plane within the liquid phase far from the vapor phase it relies on the liquid pressure P_l and the solid-liquid surface tension γ_{sl}:

$$\Sigma_x = L_y(-P_v h + 2\gamma_{sv}) = L_y(-P_l h + 2\gamma_{sl}) \qquad (2)$$

Due to translational invariance the force Σ_y exerted on a slice of fluid (vapor + liquid) in the y direction does not depend on the location of the cutting plane. It arises from the three surface tensions γ_{lv}, γ_{sl} and γ_{sv}, the liquid and vapor pressures P_l and P_v, and the line tension τ:

$$\Sigma_y = -P_v A_v - P_l A_l + l_{sv}\gamma_{sv} + l_{sl}\gamma_{sl} + l_{lv}\gamma_{lv} + 4\tau \qquad (3)$$

where A_v and A_l are the surface areas of the vapor and liquid phases in xz plane, l_{sv}, l_{sl} and l_{lv} the lengths corresponding to the intersections of respectively solid/vapor, solid/liquid and liquid/vapor interfaces with xz plane. To facilitate the determination of τ from Eq. [3] we introduce the algebraic area A_m of each meniscus region (dark blue regions in Fig. 1), from which the liquid and vapor areas write respectively $A_l = hl_{sl}/2 + 2A_m$ and $A_v = h(L_x - l_{sl}/2) - 2A_m$. The algebraic area A_m, of the same sign as $P_l - P_v$, is positive for contact angle $\theta > \pi/2$ and negative for $\theta < \pi/2$. Replacing A_l and A_v by their respective expressions and using the mechanical balance in the x direction Eq. [2], the force in the y direction simplifies without the solid/fluid surface tensions :

$$\Sigma_y = \frac{L_x}{L_y}\Sigma_x - 2A_m(P_l - P_v) + l_{lv}\gamma_{lv} + 4\tau \qquad (4)$$

As P_l, P_v and γ_{lv} are considered as uniform, the radius of curvature R, of the liquid/vapor interface, is constant. The role of the line tension τ is precisely to take into account the molecular interactions between the three phases at the vicinity of the contact line that may alter locally this uniformity[15]. From the circular geometry of the liquid vapor interface, $A_m = R^2(\beta - \sin(2\beta)/2)$ and $l_{lv}/2 = 2R\beta$ with $\beta = \theta - \pi/2$ standing for half the angle

of the arc formed by a cut in a zx plan of the confined liquid/vapor interface (blue lines in Fig. 1). In these expressions the radius of curvature $R = h/(2\sin\beta)$ is an algebraic quantity the same sign as β. Replacing A_m, l_{lv} and R by their expressions and using Laplace's law of capillarity, $P_l - P_v = 2\gamma_{lv}/R$, the force Σ_y further simplifies without pressures:

$$\Sigma_y = \frac{L_x}{L_y}\Sigma_x + \gamma_{lv} h \frac{\sin(2\beta) + 2\beta}{2\sin(\beta)} + 4\tau \tag{5}$$

Isolating τ from Eq. [5] leads to the central relation of the paper:

$$\tau = \frac{1}{2}\Sigma_m - \gamma_{lv} h K(\theta) \tag{6}$$

where the force $\Sigma_m = (\Sigma_y - \Sigma_x L_x/L_y)/2$ corresponds to the total force in the y direction acting on each meniscus region (dark blue regions, blue lines and red dots in Fig. 1). The function $K(\theta)$ is a combination of trigonometric functions, which weakly depends on the contact angle (see Fig. 2(a)):

$$K(\theta) = \frac{\sin(2\beta) + 2\beta}{8\sin(\beta)} = \frac{1}{4}\Big(\sin(\theta) - \frac{\theta - \pi/2}{\cos(\theta)}\Big) \tag{7}$$

The function K is symmetric with respect to the angle $\theta = \pi/2$ (or $\beta = 0$). The line tension τ given by Eq. [6] is thus obtained from the difference of half the total force applied on a meniscus region in the y direction, that is the total force $\Sigma_m/2$ based on line, surface and bulk contributions, minus the term $\gamma_{lv} h K(\theta)$ which stands for the force due to bulk and surfaces only.

The forces Σ_x and Σ_y are computed using the virial expression of anisotropic stresses at an unstructured solid surface from the positions of the N fluid particles[40,41]:

$$\Sigma_\alpha = \Big\langle -\frac{N k_B T}{L_\alpha} + W_\alpha \Big\rangle \tag{8}$$

with $\alpha = x, y$ and k_B Boltzmann's constant. W_α is the energy derivative relative to a homogeneous affine expansion of all the fluid atomic positions and the system boundaries in the direction α.

Unlike the forces Σ_x, Σ_y and Σ_m, line tension τ depends on the geometrical parameterization of the system. This dependence underlines that line tension is not an intrinsic parameter[42] except in the special case of a straight triple line formed by three fluids at the same pressure[19]. This 1D exception is analogous to the 2D case of the intrinsic surface tension characterizing a planar interface that separates two phases at the same pressure. In the absence of pressure uniformity (as encountered here), line and surface tensions depend on the definition of interface position[36]. This is the case if interfaces are curved or in the presence of a solid phase under non-isotropic stress for which the concept of scalar pressure must be replaced by an elastic stress tensor. Surface and line tensions are

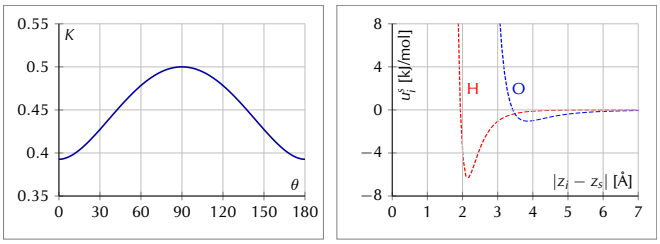

(a) (b)

Figure 2. (a) Trigonometric function $K(\theta)$ accounting for bulk and surface contributions to the meniscus free energy Σ_m. (b) Interaction potentials of the hydrogen-bonding solid used in the water simulations. The hydrogen of water is strongly attracted towards the solid, therefore mimicking a hydrogen bond interaction.

therefore dependent on the choice made to define the position of the surface and contact angle as it appears in Eq. [6] where the value of τ depends on the geometrical quantities h and θ that may be defined according to various conventions at the molecular scale.

To adopt a definition of the distance h that is based on physical parameters, we consider the surface excess Γ_l of fluid at the solid-liquid interface. The conservation of fluid mass in a vertical slab located in the liquid phase writes $2\Gamma_l + h\rho_l = n_l$ with ρ_l the bulk liquid density (see *Supplementary Information* and Fig. 3) and n_l the average number of molecules per unit of solid surface area in a slab perpendicular to the x direction taken within the liquid (inset of Fig. 3). Using the Gibbs convention, that is a zero fluid adsorption $\Gamma_l = 0$, leads to the definition of h that verifies $h = n_l/\rho_l$.

The second geometric parameter, the contact angle θ, is then deduced from Laplace's law of capillarity:

$$\cos\theta = -\frac{(P_l - P_v)h}{2\gamma_{lv}} = \frac{h}{l}\Big[\frac{1}{2\gamma_{lv}L_y}\Big(\Sigma_z + P_v L_x L_y\Big) - 1\Big] \tag{9}$$

where Σ_z, the force exerted by the fluid on the bottom solid surface, subdivides into volume and surface contributions $\Sigma_z = L_y[2\gamma_{lv} - P_l l - P_v(L_x - l)]$. This definition is self consistent with the establishment of Eqs. [6] and [7]. The so obtained contact angle incorporates disjoining pressure effects which are not, for simplicity reason, substracted to the pressure in the expression of Σ_z (see Supplementary Information 5.2). Such a definition, fully agrees with macroscopic contact angle for large pores (see Fig. 3) but leads to an effective deviation of the contact angle for strong confinement (see Fig. 4(b)). Nevertheless, it turns out that this definition leads to an efficient way to parameterize the line tension at least for LJ fluids as shown in Fig. 5.

In the end, the numerical values of γ_{sl} and γ_{sv} are not needed to extract τ as these quantities simplify in the derivation. The distance l between the two vapor/liquid menisci is defined through the zero adsorption criterion at the liquid-vapor interface: $l = [n_m - \rho_v L_x]/[\rho_l - \rho_v]$ where

n_m is the average number of fluid molecules per unit of surface area in a slab perpendicular to the z direction at the center of the slit (inset Fig. 3). The vapor pressure P_v is determined from the mean vapor density ρ_v in the middle of the dry pore region using the ideal gas law, $P_v = \rho_v k_B T$. Liquid-vapor surface tension γ_{lv} is measured in an independent simulation of an infinite planar liquid-vapor interface following the classical mechanical route (see Supplementary Information). The definition Eq. [9] of the contact angle was used as it is relevant for any confinement h and solid-fluid interaction ε_s.

B. Lennard-Jones fluid

The Lennard-Jones fluid involves repulsive and dispersive interactions with a total energy given by

$$U = \sum_{i<j} u_{ij}^f + \sum_i \sum_s u_i^s \tag{10}$$

where u_{ij}^f is the pair additive fluid interaction

$$u_{ij}^f = 4\varepsilon\Big[\Big(\frac{\sigma}{r_{ij}}\Big)^{12} - \Big(\frac{\sigma}{r_{ij}}\Big)^{6}\Big] \tag{11}$$

and u_i^s is the fluid-wall interaction

$$u_i^s = \varepsilon_s\Big[\frac{2}{15}\Big(\frac{\sigma_s}{|z_i - z_s|}\Big)^{9} - \Big(\frac{\sigma_s}{|z_i - z_s|}\Big)^{3}\Big] \tag{12}$$

with s referring to the lower or upper solid plates located at z_s ($s = l, u$), r_{ij} the distance between fluid particles i and j, z_i the z-position of fluid particle i and (ε, σ) and $(\varepsilon_s, \sigma_s)$ respectively the LJ fluid-fluid and solid-fluid interaction parameters (unless stated otherwise, $\sigma_s = 2\sigma$). The fluid-wall 9-3 interaction Eq. [12] corresponds to the regular LJ potential integrated over a half space infinite solid. A truncation cutoff radius of $r_c = 4\sigma$ is used for fluid-fluid interactions. The temperature T is constrained using a Nosé-Hoover thermostat with a damping time $t_{\text{damp}} = 100\Delta t$. In our simulation, the number of particles N varies between 560 and 18900. Each molecular dynamics simulation runs at constant volume V adjusted according to the number of particles, $42\sigma < L_x < 90\sigma$, $L_y = 21\sigma$ and $L_z = 80\sigma$. The simulations consist of 10^8 timesteps with $\Delta t = 0.005\,\sigma\sqrt{m/\varepsilon}$ (m is the mass of the particle). The forces Σ_α ($\alpha = x, y$) expressed in Eq. [8] of the main article are computed every $100\Delta t$. For post analysis, the configurations are stored every $10^4\Delta t$. Error bars are computed using the block averaging method on blocks of size $9 \times 10^6 \Delta t$, and are of the order of the symbol size in Fig. 5.

C. Water

Water molecular dynamics simulations were carried out with 480 to 3960 rigid SPC/E molecules in simulation boxes of dimensions

$$L_x = [12, 24] \text{ nm}$$
$$L_y = 4 \text{ nm}$$
$$L_z = [3.35, 3.45, 3.55, 3.65, 3.75, 3.85, 4.85, 6.15] \text{ nm}$$

The confinement parameter h defined through the zero fluid adsorption condition at the solid-liquid surface varies between 1 and 5 nm. The line tensions shown in Fig. [7] correspond to the case $L_z = 3.75$ nm and $h = 2.6$ nm. In the SPC/E model, fluid-fluid dispersive interactions are modeled using a Lennard-Jones potential with a cutoff radius of 9 Å. Electrostatic forces are computed using a cutoff radius of 9 Å coupled to a long-range correction computed through the PPPM algorithm. To avoid interactions between periodic images in the z direction, the methodology exposed in[43] is applied, inserting 3 empty boxes between the periodic images in z direction. The motion of the water molecules is integrated using a rigid-body integrator with a timestep of $\Delta t = 2$ fs. The temperature is constrained to $T = 300$ K using a Nosé-Hoover thermostat with a characteristic damping time $t_{damp} = 1$ ps. Configurations are stored every 2 ps for post-analysis. Simulations are run for a total duration of 50 ns. Error bars are computed using the block averaging method on blocks of 450 ps.

The interaction between water and the solid is either chosen to be dispersive or to involve hydrogen-bonding. In the dispersive case, only oxygen atoms interact with the solid. To model this interaction, using Eq. [12], we choose $\sigma_s = 3$ Å and ε_s is varied between 1.57 and 7.22 kJ/mol to scan a broad range of hydrophilicities. In the hydrogen-bonding case, we model the water-solid interactions through a potential:

$$u_i^s = \frac{\eta\varepsilon_s}{n-m}\Big[m\Big(\frac{\sigma_s}{|z_i - z_s|}\Big)^{n} - n\Big(\frac{\sigma_s}{|z_i - z_s|}\Big)^{m}\Big] \tag{13}$$

with $[n, m] = [12, 6]$, $\sigma_s = 3.85$ Å and $\varepsilon_s = 1.05$ kJ/mol for oxygen atoms and $[n, m] = [12, 8]$, $\sigma_s = 2.14$ Å and $\varepsilon_s = 6.36$ kJ/mol for hydrogen atoms. The parameter η is varied between 1 and 5.25 to scan a broad range of hydrophilicities. This would correspond, for real polar sites, to a variation of site density on the solid surface. The interaction potential with $\eta = 1$ is shown in Fig. 2(b). This interaction potential is inspired by similar potentials calibrated in the case of atomically structured solids to model H-bonding. Yoshida et al.[44] proposed the potential described by Eq. [13] to model the interatomic interactions between the atoms of the first solid layer and the water molecules using a parameter $\eta = 2.34$.

III. RESULTS

Molecular dynamics simulations were performed using LAMMPS[45]. We considered the strategy above to determine τ for the prototypical LJ fluid (parameters ε and σ). Full details regarding the molecular simulations can

be found in *Materials and Methods* and *Supplementary Information*.

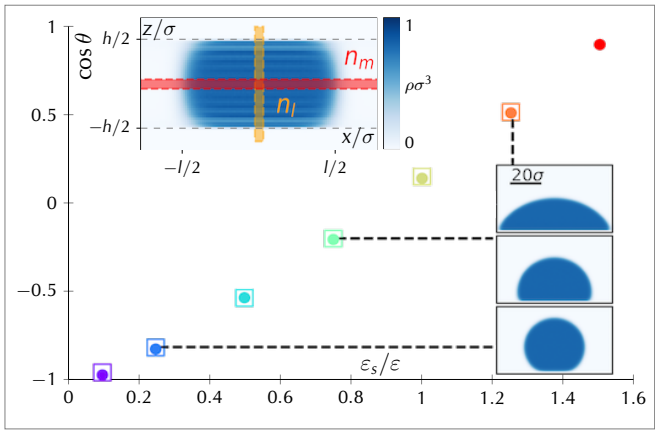

Figure 3. Contact angles θ obtained for a Lennard-Jones fluid from Eq. [9] for large confinements (filled circles) or from shape regression for large hemicylinders (empty squares, right insets, see *Supplementary Information*). Contact angles are plotted according to the ratio of the fluid/solid to the fluid/fluid interaction strengths $\varepsilon_S/\varepsilon$ (values increasing from purple to red). The top inset shows the density of the structured fluid in blue with the yellow and red areas denoting the regions used to define the confinement h and the meniscus separation l (these regions contain n_l and n_m molecules, respectively, see text).

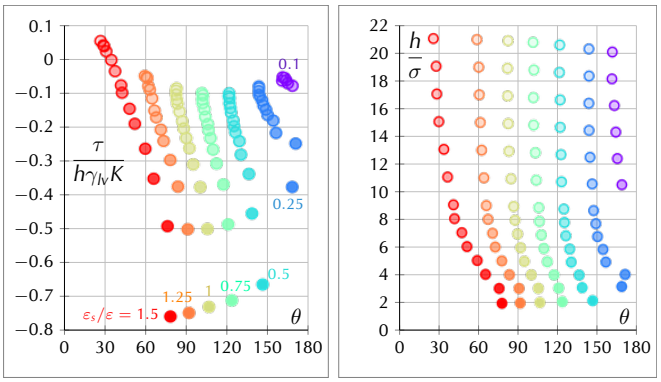

(a) (b)

Figure 4. (a) Dimensionless ratio of the line tension τ over the total force $h\gamma_{sl}K$ due to bulk and surface contributions for several fluid/solid to fluid/fluid interaction strength ratio $\varepsilon_s/\varepsilon$ increasing from purple to red. For a given color, the intensity from opaque to transparent indicates increasing h. (b) Dependence of the contact angle θ on the relative confinement h/σ according to the interaction strength ratio (colors).

As shown in Fig. 3, $\cos\theta$ determined using Eq. [9] follows the expected linear dependence on ε_s[46] and, for large h, agrees with contact angles measured through the shape regression technique of fluid density maps. The contact angle as defined by Eq. [9] is however not only dependent on the wall/fluid interaction strengths but also on other physical and geometrical parameters such as the confinement (Fig. 4(b)). This variation emerges from the dependence of solid/vapor and solid/liquid surface tensions on the separation h due to solid-fluid-solid interactions and adsorption effects (see *Supplementary Information*). In particular, solid-fluid-solid interactions induce a significant increase of the contact angle when perfectly wetting surfaces are brought together.

Different wall/fluid interaction strengths ε_s, confinements h and temperatures T were considered to probe the value of the line tension τ on a broad range of parameters for the LJ fluid. At the higher considered temperature, of the order of 0.7 times the critical temperature, the error on the vapor pressure P_v given by the perfect gas law is smaller than 5%[47]. We checked for each parameter set, that the magnitude of τ is significantly larger than the fluctuations on each of the two terms used in the difference in Eq. [6] to extract τ (see Supplementary Information and Fig. S3). Moreover, as shown in Fig. 4(a), in most considered cases τ is larger than 10% of the last term of Eq. [6] which fully legitimizes its measurement from the difference between the two terms of Eq. [6]. Among the various considered cases, an important variability in the line tension values is observed. However, as shown in Fig. 5, all line tension values almost collapse on a single master curve when plotted according to the contact angle θ extracted for each set of parameters. Despite the large range of values explored for each parameter the limited departure from this general trend is particularly unexpected. The collapse of τ on a single curve for different ε_s, σ_s, T and h suggests that, to first order, the line tension can be estimated using θ only. This parameterization is possible when using the zero adsorption definition for h and the corresponding definition for θ given in Eq. [9].

The line tension plotted according to the contact angle demonstrates a non monotonic behavior with a minimum negative value for τ around $\theta = 90°$and a divergence towards positive values close to the wetting transition. This behavior makes the bridge between nonlocal Density Functional Theory (DFT) calculations[17] (dashed line in Fig. 5) and Interface Displacement Model (IDM) by Joanny and de Gennes[15] (solid line in Fig. 5) at the wetting transition. At the dewetting transition $\theta \to 180°$, the vapor wedge separating the liquid from the solid vanishes together with its contact line and its associated free energy τ. For intermediate solid/fluid interaction strengths $0° < \theta < 180°$, the line tension is driven by a combination of microscopic effects that arise from the competition between the different molecular interactions but also potentially from fluid layering at interfaces. Here, analytic sums over molecular interactions do not allow estimating τ as it corresponds to a free energy contribution that also includes an entropy term[48]. For $\theta = 90°$, τ can be seen as a correction of the liquid-vapor surface tension which accounts for the progressive vanishing of pressure anisotropy close to the solid surface. This reduced pressure anisotropy lowers

the free energy cost related to the liquid-vapor interface so that τ is negative (as discussed in *Supplementary Information*, $\tau(90^\circ) \sim -\gamma_{lv}\sigma = -0.74\varepsilon/\sigma$). At the wetting transition $\theta \to 0^\circ$, liquid-vapor and solid-liquid interfaces become parallel and close to each other in the vicinity of the contact line. In this configuration, the line tension τ is mainly controlled by the disjoining pressure which arises from the interaction between these two interfaces. In this case, the IDM[15] predicts that the line tension diverges as $\tau = \gamma_{lv} a(\ln(1/\theta) - 1)$ with a a solid-fluid interaction length (see *Supplementary Information*). The molecular simulation data in Fig. 5 are consistent with the divergence predicted at the wetting transition by the IDM (solid line in Fig. 5).

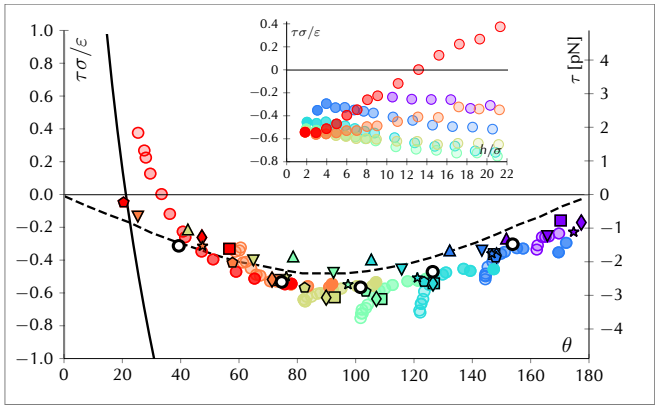

Figure 5. Line tension τ for a LJ fluid confined in slit pores of width h ranging from 2 to 21 σ. For a given h, different interaction strengths ε_s are considered (same color code as in Figs. 3 and 4). For a given color, the intensity from opaque to transparent indicates increasing h (see inset showing τ as a function of h for different ε_s). Different T were considered: $k_B T/\varepsilon = 0.7$ □, 0.75 ◇, 0.85 ⬠, 0.9 ★, 0.95 ▽, and 1.0 △. The dashed line represents a nonlocal DFT model in a wedge[17]. The solid line corresponds to the Interface Displacement Model at the wetting transition[15]. Simulations with $\sigma_s = \sigma$ lead to a similar behavior (black circles). Right axis: same τ but in real units using LJ parameters for argon ($\sigma = 3.4$ Å, $\varepsilon/k_b = 120$ K).

For wetting surfaces $\theta < 90^\circ$, the effect of confinement on line tension provides evidence for the limitation of the scaling methodology based on Eq. [1] (inset of Fig. 5). Line tensions are sometimes assumed to correspond to the curvature dependence of the liquid-vapor surface tension described through the Tolman length[33,34]. Yet, a major difference between effects arising from the stress anisotropy close to the contact line and curvature effects lies in the the spatial distribution of the excess free energy. While τ corresponds to effects localized in the vicinity of the contact line, curvature effects are distributed over the whole liquid-vapor interface (meniscus). Fig. 6(a) shows an estimate of the distribution of local stress anisotropy $p_y - p_x$ and local excess free energy $\varphi(x,z)$ with respect to the bulk and surface value for a representative example $\theta \sim 90^\circ$(local stresses were obtained from post-processing of the simulation following the Irving-Kirkwood convention[49]). Fig. 6(b) shows that the excess free energy $\phi(z)$, obtained from the integration of $\varphi(x,z)$ along the x direction, is strongly localized close to the triple lines, therefore supporting the line tension concept (see *Supplementary Information* for computation details).

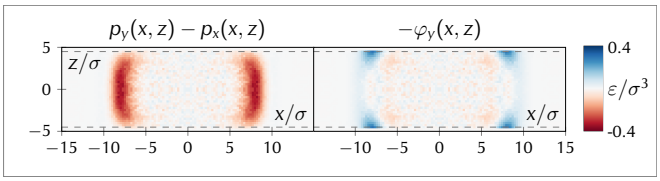

(a)

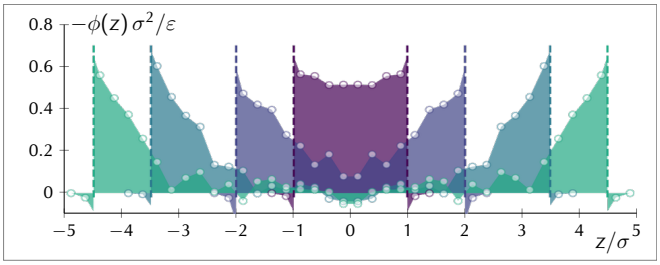

(b)

Figure 6. (a) Local pressure anisotropy $p_x - p_y$ and excess free energy $\varphi(x,z)$ for a LJ fluid confined in a slit pore. The solid-fluid interaction strength ε_s was chosen so that $\theta = 96^\circ$. (b) Distribution of the excess free energy $\phi(z)$ obtained as the integral along x of $\varphi(x,z)$. Each color plot corresponds to a different h which increases from purple to green. The colored areas, which represent the integral of the excess free energy along the z direction, correspond to 2τ.

The novel strategy presented here was also used to determine the line tension τ for water (SPC/E water model) in the vicinity of structureless solid surfaces which interact with water through dispersive interactions or through homogeneously distributed hydrogen bonding[44] (see *Materials and Methods* and[44]). Measurements are done at room temperature $T = 300$ K at which the water vapor is well modeled as a perfect gas. Wall-induced polarization effects, ignored with the first type of interaction, are taken into account with the second type of interaction which mimics proton-acceptor sites of real surfaces. Fig. 7 shows τ for water as a function of θ for both solid surfaces to investigate the effect of the molecular interactions at play. The two data sets feature a non monotonic behavior similar to that observed for the Lennard-Jones fluid. In both cases τ is minimum around 90°and vanishes at the dewetting transition $\theta \to 180^\circ$. This general non monotonic behavior suggests that the unifying formalism, described earlier for the LJ fluid, can be used for various fluids and solid/fluid interactions.

However, an important difference is observed at the wetting transition $\theta \to 0^\circ$. The line tension τ for water close to dispersive surfaces becomes positive and diverges

while it converges to a finite, seemingly negative, value for hydrogen-bonding surfaces. In view of the difference between the two interaction types, it is tempting to qualitatively relate such a behavior to the theoretical predictions of Indekeu[15,50] in the framework of the IDM. In the dispersive case, characterized by z^{-3} attractive interactions between the solid and oxygen atoms of water, like for the LJ fluid, a divergence of the line tension at wetting is predicted. In the hydrogen-bonding case, water interactions with the solid differ in terms of oxygen/solid and hydrogen/solid interactions. Attractive interactions of oxygen and hydrogen atoms with solid plates scale respectively as z^{-6} and z^{-8} (see Fig. 2(b)). In both cases, these interactions decay faster than those corresponding to Van der Waals interactions (see Fig. 2(b)) so that they can be referred to short-range interactions according to Indekeu's formalism. The IDM model predicts for such short-range fluid/solid interactions that the line tension converges towards a finite and positive value. The fact that a finite line tension is measured at the wetting transition in the hydrogen bonding case suggests that it is indeed mainly controlled by these so called short-range interactions when $\theta \to 0°$.

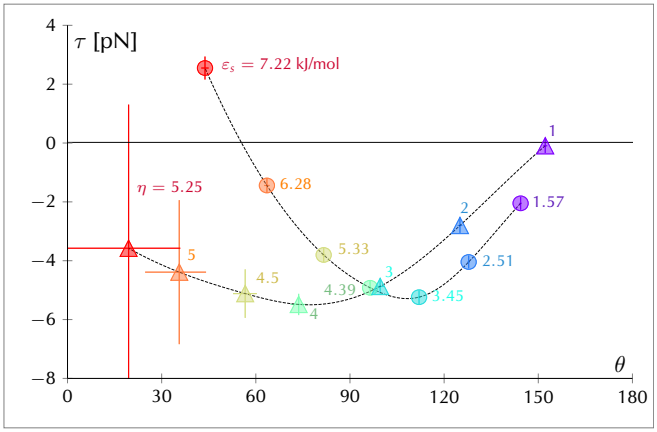

Figure 7. Line tension τ for water confined at room temperature ($T = 300$ K) in a slit pore of a width $h = 2.6$ nm between dispersive (circles) and hydrogen bonding (triangles) surfaces. For dispersive surfaces, the hydrophilicity is controlled by the solid-liquid interaction strength ε_s. For hydrogen bonding surfaces, the hydrophilicity is controlled by the parameter η (see *Materials and Methods*).

The line tension tension in the case of water confined between either of the two types of surfaces is found to be about -5 pN for a contact angle close to 90°. This value, measured at room temperature, is comparable with the value of -11 pN extracted by Tinti et al from a simulation of a bubble nucleation within a hydrophobic cylindrical nanopore corresponding to a contact angle of 119°[3]. The similarity between these two line tension values is remarkable given the strong difference between the two numerical approaches. Here we study a straight contact line at equilibrium, while Tinti et al study an out of equilibrium nucleation during which the contact line is presumably submitted to strong variations in term of geometry and curvature. The factor of 2 between the two numerical values could reflect a sensitivity of the line tension to curvature. It could also be a due to the difference between the solid (smoth flat wall versus atomistic cylindrical wall) and the numerical water model (SPC/E versus TIP4P) at play in the tow studies. Our results with SPCE/E water suggest indeed that the nature of the solid may have an impact on the line tension. Although the negative extremum value of the line tension is similar for the two solids we considered, the extremal values are obtained at different contact angles. Nevertheless a factor of 2 between our value and Tinti's value is not so large when considering the range of values, covering several order of magnitude, that is found in the literature. Even more striking is the proximity of these values with the experimental value of -25 pN deduced from the experimental measurement of the extrusion pressure of pure real water out from hydrophobic nanopores (silica grafted cylinders) having a similar contact angle[1]. Again the difference in the nature of the solid and of the liquid as well as the nature of the system, straight contact line versus curved out of equilibrium contact line, could explain the difference between the three measured values.

IV. CONCLUSION

This study sheds light on the concept of line tension. It unravels a generic behavior, with in the case of dispersive fluids, a main dependence on the contact angle only. Using a novel strategy relying on a mechanical measurement at the molecular scale, our data for the Lennard-Jones fluid and water provide robust line tensions which depend on the wetting properties of the solid surface by the liquid phase. Our line tension values are found to be consistent with a series of theoretical, numerical and experimental data.

The generic behavior emerging from our data, established on a full range of contact angles, allows unifying the different, sometimes conflicting, pictures in the literature. Far from the wetting transition, the line tensions inferred from our analysis suggest that this concept is robust down to the molecular scale with a simple dependence on confinement, temperature and solid-fluid interaction encompassed in the contact angle. For a contact angle about 90°, the line tension for water at room temperature is consistent with that inferred from out of equilibrium numerical and experimental measurements based on water extrusion from hydrophobic porous materials. Beyond measuring line tension values, the computational approach is particularly useful to identify the molecular structures, which are not accessible experimentally, such as layering, adsorption, presence of chemical groups such as OH^- responsible for the measured line tension. While the present study is limited to a single liquid/vapor system at equilibrium on unstructured solid surfaces, additional physical features are to be expected for structured

and thermalized surfaces, fluid mixtures, and out of equilibrium processes such as bubble nucleation.

ACKNOWLEDGMENTS

This work was supported by the French Research Agency (ANR TAMTAM 15-CE08-0008 and LyStEn 15-CE06-0006). We thank E. Charlaix for fruitful discussions and NVIDIA Corporation for the donation of a Tesla K40 GPU used for this research.

REFERENCES

[1]L. Guillemot, T. Biben, A. Galarneau, G. Vigier, and E. Charlaix, "Activated drying in hydrophobic nanopores and the line tension of water," Proc. Nat. Acad. Sci. **109**, 19557–19562 (2012).
[2]R. C. Remsing, E. Xi, S. Vembanur, S. Sharma, P. G. Debenedetti, S. Garde, and A. J. Patel, "Pathways to dewetting in hydrophobic confinement," Proc. Nat. Acad. Sci. **112**, 8181–8186 (2015).
[3]A. Tinti, A. Giacomello, Y. Grosu, and C. M. Casciola, "Intrusion and extrusion of water in hydrophobic nanopores," Proc. Natl. Acad. Sci. , 20266–10273 (2017).
[4]V. Satarifard, A. Grafmüller, and R. Lipowsky, "Nanodroplets at Membranes Create Tight-Lipped Membrane Necks via Negative Line Tension," ACS Nano **12**, 12424–12435 (2018).
[5]P. G. de Gennes, "Wetting: statics and dynamics," Rev. Mod. Phys. **57**, 827–863 (1985).
[6]D. Bonn, J. Eggers, J. Indekeu, J. Meunier, and E. Rolley, "Wetting and spreading," Rev. Mod. Phys. **81**, 739–805 (2009).
[7]R. Lhermerout and K. Davitt, "Contact angle dynamics on pseudo-brushes : Effects of polymer chain length and wetting liquid," Colloids Surfaces A **566**, 148–155 (2019).
[8]D. Lohse and X. Zhang, "Surface nanobubbles and nanodroplets," Rev. Mod. Phys. **87**, 981–1035 (2015).
[9]F. Bresme and N. Quirke, "Computer Simulation Study of the Wetting Behavior and Line Tensions of Nanometer Size Particulates at a Liquid-Vapor Interface," Phys. Rev. Lett. **80**, 3791–3794 (1998).
[10]H. Tan, H. An, and C.-d. Ohl, "Resolving the Pinning Force of Nanobubbles with Optical Microscopy," Phys. Rev. Lett. **054501**, 1–5 (2017).
[11]Y. Singh, J. Gopal, K. Raval, F. Ali, M. Chaurasia, N. K. Jain, and M. K. Chourasia, "Nanoemulsion : Concepts , development and applications in drug delivery," J. Control. Release **252**, 28–49 (2017).
[12]M. K. Debe, "Electrocatalyst approaches and challenges for automotive fuel cells," Nature **486**, 43–51 (2012).
[13]T. G. Karayiannis and M. M. Mahmoud, "Flow boiling in microchannels : Fundamentals and applications," Appl. Therm. Eng. **115**, 1372–1397 (2017).
[14]R. D. Deegan, O. Bakajin, T. F. Dupont, G. Huber, S. R. Nagel, and T. A. Witten, "Capillary flow as the cause of ring stains from dried liquid drops," Nature **389**, 827–829 (1997).
[15]J. Joanny and P. De Gennes, J. Colloid Interface Sci..
[16]J. Drelich, "The significance and magnitude of the line tension in three-phase (solid-liquid-fluid) systems," Colloids Surfaces A Physicochem. Eng. Asp. **116**, 43–54 (1996).
[17]J. H. Weijs, A. Marchand, B. Andreotti, D. Lohse, and J. H. Snoeijer, "Origin of line tension for a Lennard-Jones nanodroplet," Phys. Fluids **23**, 022001 (2011).
[18]J. W. Gibbs, "On the equilibrium of heterogeneous substances," (1876).
[19]J. S. Rowlinson and B. Widom, *Molecular Theory of Capillarity* (Clarendon Press, Oxford, 1982).
[20]J. Y. Wang, S. Betelu, and B. M. Law, "Line tension effects near first-order wetting transitions," Phys. Rev. Lett. **83**, 3677–3680 (1999).
[21]T. Pompe and S. Herminghaus, "Three-phase contact line energetics from nanoscale liquid surface topographies," Phys. Rev. Lett. **85**, 1930–1933 (2000).
[22]A. Checco, P. Guenoun, and J. Daillant, "Nonlinear Dependence of the Contact Angle of Nanodroplets on Contact Line Curvature," Phys. Rev. Lett. **91**, 186101 (2003).
[23]N. Kameda and S. Nakabayashi, "Size-induced sign inversion of line tension in nanobubbles at a solid/liquid interface," Chemical Physics Letters **461**, 122 – 126 (2008).
[24]J. K. Berg, C. M. Weber, and H. Riegler, "Impact of Negative Line Tension on the Shape of Nanometer-Size Sessile Droplets," Phys. Rev. Lett. **105**, 076103 (2010).
[25]S. P. McBride and B. M. Law, "Influence of line tension on spherical colloidal particles at liquid-vapor interfaces," Phys. Rev. Lett. **109**, 196101 (2012).
[26]L.-O. Heim and E. Bonaccurso, "Measurement of line tension on droplets in the submicrometer range," Langmuir **29**, 14147–14153 (2013), pMID: 24156499.
[27]T. Werder, J. H. Walther, R. L. Jaffe, T. Halicioglu, and P. Koumoutsakos, "On the water-carbon interaction for use in molecular dynamics simulations of graphite and carbon nanotubes," The Journal of Physical Chemistry B **107**, 1345–1352 (2003).
[28]J. T. Hirvi and T. A. Pakkanen, "Molecular dynamics simulations of water droplets on polymer surfaces," J. Chem. Phys. **125**, 144712 (2006).
[29]D. Winter, P. Virnau, and K. Binder, "Monte carlo test of the classical theory for heterogeneous nucleation barriers," Phys. Rev. Lett. **103**, 225703 (2009).
[30]J. Zhang, F. Leroy, and F. Müller-Plathe, "Influence of Contact-Line Curvature on the Evaporation of Nanodroplets from Solid Substrates," Phys. Rev. Lett. **113**, 046101 (2014).
[31]B. M. Law, S. P. McBride, J. Y. Wang, H. S. Wi, G. Paneru, S. Betelu, B. Ushijima, Y. Takata, B. Flanders, F. Bresme, H. Matsubara, T. Takiue, and M. Aratono, "Line tension and its influence on droplets and particles at surfaces," Progress in Surface Science **92**, 1 – 39 (2017).
[32]M. N. Joswiak, N. Duff, M. F. Doherty, and B. Peters, "Size-dependent surface free energy and tolman-corrected droplet nucleation of tip4p/2005 water," The Journal of Physical Chemistry Letters **4**, 4267–4272 (2013).
[33]M. Kanduč, "Going beyond the standard line tension: Size-dependent contact angles of water nanodroplets," J. Chem. Phys. **147**, 174701 (2017).
[34]S. K. Das, S. A. Egorov, P. Virnau, D. Winter, and K. Binder, "Do the contact angle and line tension of surface-attached droplets depend on the radius of curvature?" J. Phys.: Condens. Matter **30**, 255001 (2018).
[35]L. Boruvka and A. W. Neumann, "Generalization of the classical theory of capillarity," J. Chem. Phys. **66**, 5464–5476 (1977).
[36]C. A. Ward and J. Wu, Phys. Rev. Lett..
[37]A. Marmur, "Line Tension and the Intrinsic Contact Angle in Solid–Liquid–Fluid Systems," J. Colloid Interface Sci. **186**, 462–466 (1997).
[38]P. Tarazona and G. Navascués, "A statistical mechanical theory for line tension," The Journal of Chemical Physics **75**, 3114–3120 (1981).
[39]M. Shao, J. Wang, and X. Zhou, Sci. Rep..
[40]P. Schofield, J. R. Henderson, and J. S. Rowlinson, "Statistical mechanics of inhomogeneous fluids," Proceedings of the Royal Society of London. A. Mathematical and Physical Sciences **379**, 231–246 (1982).
[41]A. P. Thompson, S. J. Plimpton, and W. Mattson, "General formulation of pressure and stress tensor for arbitrary many-body interaction potentials under periodic boundary conditions," J. Chem. Phys. **131**, 154107 (2009).
[42]L. Schimmele, M. Napiórkowski, and S. Dietrich, "Conceptual

aspects of line tensions," J. Chem. Phys. **127**, 164715 (2007).
[43]I.-C. Yeh and M. L. Berkowitz, "Ewald summation for systems with slab geometry," J. Chem. Phys. **111**, 3155–3162 (1999).
[44]H. Yoshida, H. Mizuno, T. Kinjo, H. Washizu, and J.-L. Barrat, "Molecular dynamics simulation of electrokinetic flow of an aqueous electrolyte solution in nanochannels," J. Chem. Phys. **140**, 214701 (2014).
[45]S. Plimpton, "Fast Parallel Algorithms for Short-Range Molecular Dynamics," J. Compu. Phy. **117**, 1–19 (1995).
[46]R. Evans, M. C. Stewart, and N. B. Wilding, Phys. Rev. Lett..
[47]A. Schlaich and B. Coasne, "Dispersion truncation affects the phase behavior of bulk and confined fluids: Coexistence, adsorption, and criticality ," J. Chem. Phys. **154104** (2019), 10.1063/1.5085431.
[48]T. Getta and S. Dietrich, "Line tension between fluid phases and a substrate," Phys. Rev. E **57**, 655–671 (1998).
[49]J. H. Irving and J. G. Kirkwood, "The Statistical Mechanical Theory of Transport Processes. IV. The Equations of Hydrodynamics," J. Chem. Phys. **18**, 817–829 (1950).
[50]J. Indekeu, "Line tension near the wetting transition: results from an interface displacement model," Phys. A. **183**, 439–461 (1992).